

Article

Improvement of the Crack Propagation Resistance in an $\alpha + \beta$ Titanium Alloy with a Trimodal Microstructure

Changsheng Tan ^{1,*}, Yiduo Fan ¹, Qiaoyan Sun ² and Guojun Zhang ^{1,*}

¹ School of Materials Science and Engineering, Xi'an University of Technology, Xi'an 710048, China; 2190120044@stu.xaut.edu.cn

² State Key Laboratory for Mechanical Behavior of Materials, Xi'an Jiaotong University, Xi'an 710049, China; qysun@xjtu.edu.cn

* Correspondence: cstan@xaut.edu.cn (C.T.); zhangguojun@xaut.edu.cn (G.Z.); Tel.: +86-29-82668614 (C.T.); Fax: +86-29-82663453 (C.T.)

Received: 9 July 2020; Accepted: 31 July 2020; Published: 6 August 2020



Abstract: The roles of microstructure in plastic deformation and crack growth mechanisms of a titanium alloy with a trimodal microstructure have been systematically investigated. The results show that thick intragranular α lath and a small number of equiaxed α phases avoid the nucleation of cracks at the grain boundary, resulting in branching and fluctuation of cracks. Based on electron back-scattered diffraction, the strain partition and plastic deformation ahead of the crack tip were observed and analyzed in detail. Due to the toughening effect of the softer equiaxed α phase at the grain boundary, crack arresting and blunting are prevalent, improving the crack growth resistance and generating a relatively superior fracture toughness performance. These results indicate that a small amount of large globular α phases is beneficial to increase the crack propagation resistance and, thus, a good combination of mechanical property is obtained in the trimodal microstructure.

Keywords: titanium alloy; trimodal microstructures; strain partition; crack propagation

1. Introduction

Due to their high strength, good corrosion and fatigue resistance, titanium alloys have been extensively used for aerospace engineering [1,2]. During applications in the aircraft industry, two typical microstructures of bimodal microstructure and lamellar microstructure are widely used for titanium alloys [2,3]. Generally, the crack growth resistance is significantly influenced by the volume fraction and size of the equiaxed α phase as well as the grain boundary [4–6] in bimodal microstructures and equiaxed microstructures. The propagation of microvoids can be restricted by softer coarse α particles [7]. For titanium alloys, this is significantly strengthened by the fine secondary α phase [3,8]; crack growth is mainly affected by the thickness of the lamellar α phase, grain boundary α (GB α) and the α colony size of the lamellar microstructure [4,9]. High fracture toughness could be achieved in a lamellar microstructure with large α plates and the finest lamellar spacing [10–12]. It has been reported [11,13,14] that α plates are an effective microstructure unit for controlling fracture toughness as they can effectively deflect the crack propagation path. In conclusion, the fracture toughness of titanium alloy is extremely sensitive to microstructural parameters, such as the prior β grain size, α morphology, the width of the grain boundary of α phase and α laths and so on. It has been found that the lamellar shape of α phase promotes high toughness, while an equiaxed α phase results in low toughness; however, the ductility is degraded with the lamellar α phase and improved with the equiaxed α phase [15]. Due to these contradictions, the microstructure that has high fracture toughness may lead to an unsatisfactory decrease in other properties.

Recently, a new type of microstructure, named “trimodal microstructure”, has been reported. This microstructure contains a primary globular α phase, a lamellar α phase and a transformed β matrix (β_{trans} : secondary α phase and β phase) [16,17]. Hosseini et al. [18] found that the excellent comprehensive mechanical properties of the trimodal microstructure are achieved when compared with the widmanstätten microstructure and bimodal microstructure. However, there is little investigation of the deformation behavior ahead of the crack tip, crack formation and crack growth in the trimodal microstructure during loading. Especially in the two-phase titanium alloy with high strength and toughness.

Therefore, in this work, research on the plastic deformation ahead of the crack tip as well as on the detailed essential relationship between microstructure and crack propagation behavior of the Ti-6Al-2Sn-2Zr-3Mo-1Cr-2Nb-0.1Si titanium alloy with the trimodal microstructure was carried out systematically. The present results can be applied to predict the microstructural features that are required to obtain the desired mechanical properties.

2. Experimental Program

The initial titanium alloy was supplied by the Northwest Institute for Non-ferrous Metals Research of China. The ingot with diameter of 450–500 mm was obtained after 3 vacuum-consumable electric arc smelting processes. Subsequently, forging was performed more than a dozen times on the ingot and then the bar with a diameter of about 350 mm was obtained after forging. The titanium alloy was finally forged in a two-phase region of 30–50 °C (lower than the phase transition point), and it was then strengthened with a solution and aging treatment. Vacuum smelting can remove defects and obtain component uniformity. The chemical composition (wt.%) of H and O was 0.001% and 0.075%. The content of C was low than 0.005%. In present work, the phase transition temperature (T_{β}) was determined by the metallographic method with continuous heating. The α to β transformation temperature was about 945 ± 5 °C. Firstly, these samples were heated at 930 °C for 2 h and then air cooled. Several primary equiaxed α grains (α_p) were retained and some α laths with 0.5 to 1 μm in width were obtained during this process. Then, the low temperature aging at 600 °C for 4 h was performed and cooled by air to room temperature. This process was performed to obtain the secondary α precipitation from the residual β matrix. Consequently, a tri-modal microstructure (TM) was developed consisting of an intermixture of primary equiaxed α grains (α_p), α lath (α_l) and a transformed β matrix (secondary α phase (α_s) in the β matrix). A plate-shaped tensile specimen (width: 6 mm; thickness: 2 mm; gage length: 15 mm) was determined according to the national standard of the People’s Republic of China (GB/T 228-2010) and performed on INSTRON 1195 Testing Machine (INSTRON, Boston, MA, USA). At least three individual tests were carried out to increase the accuracy of the tensile property. The compact tensile specimens with a size of 25 mm \times 60 mm \times 62.5 mm were used in the present work. After the corresponding heat treatment, the specimens with a notch of a “V” shape were machined into the compact tensile specimens. Firstly, a prefabricated crack of 2 mm in length was carried out on MTS 810 machines with sinusoidal waveforms at room temperature (a stress ratio of $R = 0.1$). The tensile test was carried out on the Instron 5895 testing machine (INSTRON, Boston, MA, USA). Three specimens were carried out to increase the accuracy of K_{IC} . Finally, scanning electron microscopy (SEM, HITACHI SU6600, Tokyo, Japan) were applied to observe the fractographic surface and analyze the crack growth behavior. The microstructures were etched by a corrosion solution of $\text{HF}:\text{HNO}_3:\text{H}_2\text{O} = 1:2:5$. The microstructures ahead of the crack tip were investigated in detail using a field emission gun SEM (Carl Zeiss Microscopy GmbH 73447, Carl Zeiss AG, Jena, Germany) equipped with an electron backscattered diffraction (EBSD) system.

3. Results

3.1. Microstructures before Deformation

Figure 1 displays the SEM microstructural features before deformation of the TM. The TM contains three different α morphologies, namely, the equiaxed primary α phase (α_p), the lamellar α phase (α_l) and the acicular secondary α phase (α_s), as shown in Figure 1a. A few α_p are located at the prior β grain boundary. Figure 1b displays the magnified image of the morphology of α_l and α_s in the β_{trans} matrix, as indicated by the blue box. The grain size, volume fraction and aspect for α_p are about 5.9 μm , 5.0% and 1.5, respectively. The thickness for α_l and α_s is about 554 nm and 133 nm, respectively. The volume fraction for α_l and the β_{trans} matrix is about 32.0% and 62.0%, respectively.

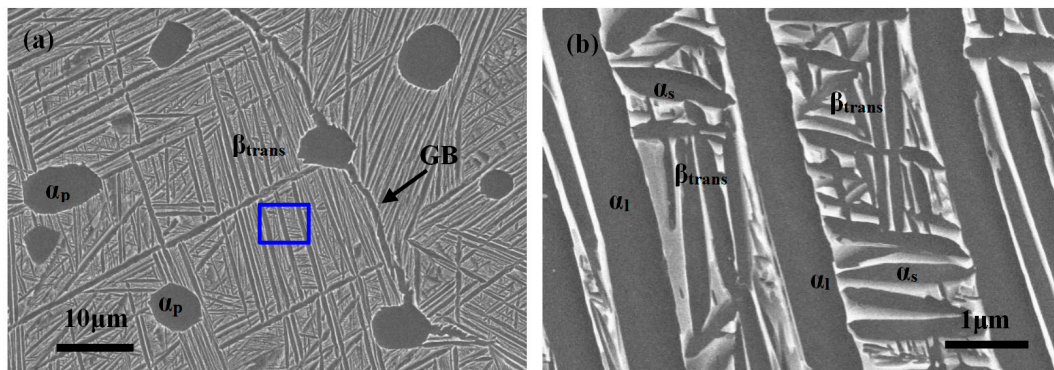


Figure 1. The SEM features of the trimodal microstructure (TM) before deformation: (a) three different α morphologies, namely, the primary equiaxed α phase (α_p), the lamellar α phase (α_l) and the secondary α phase (α_s); (b) the morphology of α_l and α_s in the β_{trans} matrix.

3.2. Mechanical Properties of the Alloy with a TM

The tensile engineering stress–strain curves at room temperature of the TM are shown in Figure 2a, which indicates that the average value of yield strength, tensile strength and elongation of the TM are about 1067 MPa, 1186 MPa and 12.1%, respectively. Figure 2b displays the force–displacement curve. The fracture toughness of the TM is approximately 62 $\text{MPa}\cdot\text{m}^{1/2}$ and is significantly higher than the bimodal microstructure and bi-lamellar microstructure [19], which indicates that a small number of the equiaxed primary α phases are beneficial to the improvement of fracture toughness. The mechanical properties and the error of these measurements are listed in Table 1. It can be concluded that a good comprehensive mechanical property is achieved for the TM in the present work, which has been reported in other studies [16,18].

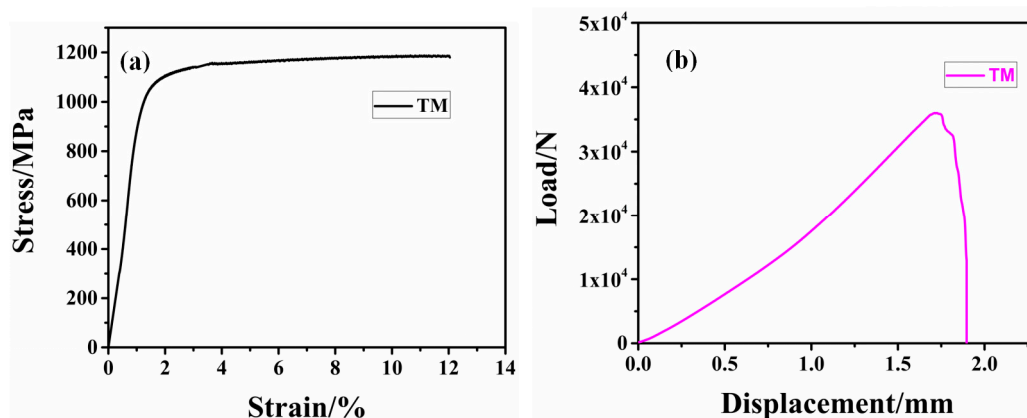


Figure 2. The comparison of mechanical properties of the TM and BLM: (a) the engineering stress–strain curves; (b) the force–disposition curves.

Table 1. The mechanical properties of the bimodal microstructure and bi-lamellar microstructure.

Microstructures	Yield Strength/MPa	Tensile Strength/MPa	Elongation/%	Fracture Toughness/MPa·m ^{1/2}
TM	1067 ± 24	1186 ± 4	12.1 ± 1	62 ± 1

3.3. Fractographic Analyses and the Crack Propagation Behavior

The characteristics of fracture surfaces will provide important information to clarify the fracture mechanism during the failure process. To reveal the influence of the microstructure on the fracture mechanisms, the samples with different combinations of α phase were opted for the fracture analysis. Fracture morphology of the TM is shown in Figure 3. As can be seen, the fracture surface could be clearly separated into two apparent zones the: crack source zone and crack growth zone (Figure 3a). To further observe the detailed information regarding the fracture surface, some local fractographs of the TM were obtained, as shown in Figure 3.

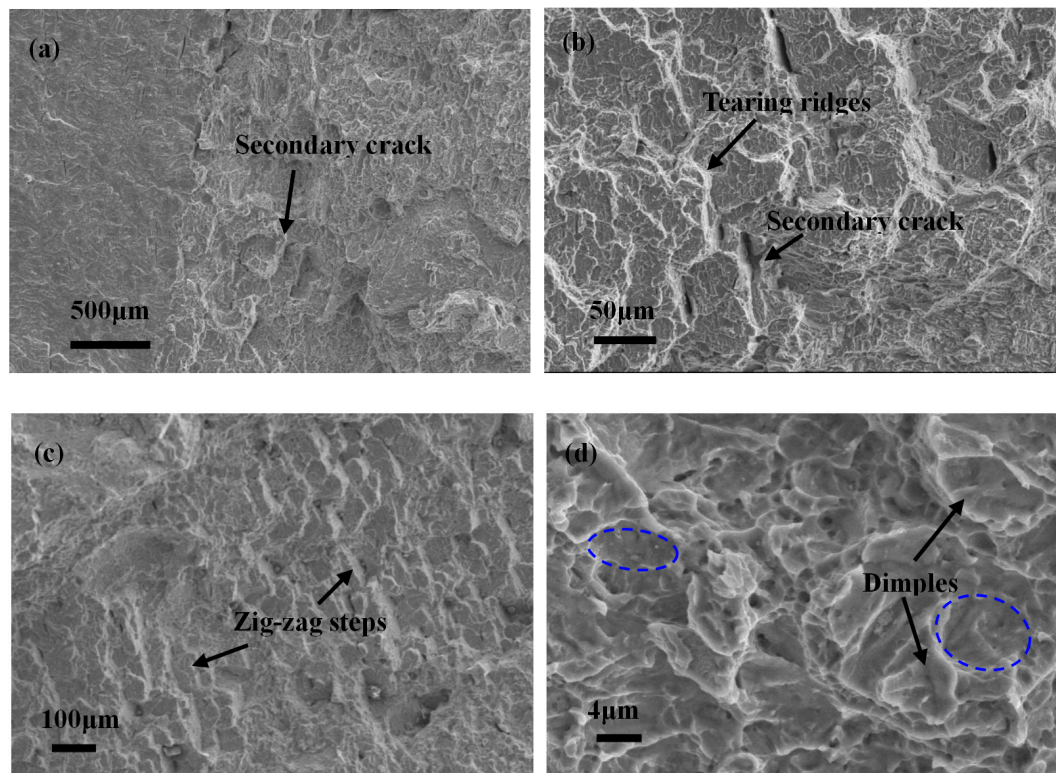


Figure 3. The SEM morphological characteristics of the fracture toughness of the TM fractures: (a) the transition region from fatigue crack to tensile crack propagation, (b) tear ridges and secondary cracks, (c) large fracture steps with a zig-zag fracture pattern, (d) big dimples surrounded by ridges.

The fracture surface of the TM is characterized by a high amount of ductile tearing ridges and secondary cracks resulting in transgranular crack propagation of the whole crack propagation region, which indicates a dimple-type fracture (ductile fracture), as shown in Figure 3a,b. The large number of tearing ridges that appear on the fracture surface and the fibrous zones imply a transgranular fracture (Figure 3b), which has previously been reported in titanium alloy [3,20]. The fracture toughness can be improved by the tearing ridges, which indicates that the higher the number of ridges, the higher the achievable K_{IC} of the titanium alloy [21]. Furthermore, a large amplitude of fracture steps with zig-zag fracture patterns are present in the crack propagation region (Figure 3c), which indicates that the crack alters direction and causes crack bifurcation, zigzagging and formation of secondary cracks, that is, much more fracture energy is consumed [22,23]. Thus, it can be concluded that the considerable steps

were induced by large crack deviation. Figure 3d exhibits a significant number of inhomogeneous and deep ductile dimples and microvoids, which reveals that the fracture is caused by the typical ductile mechanism of microvoid nucleation, growth, and coalescence [24].

It has been reported that the fracture toughness was mainly affected by the tortuosity of the crack path and plastic deformation ahead of the crack tip [25]. In general, the improvement in tortuosity and plasticity is beneficial to the process of enhancing the fracture toughness of material [26]. The crack front profiles of the fractured specimen of TM are shown in Figure 4. Figure 4a is the main crack propagation path of the TM. The letters b, c, d and e denote the regions that are selected for detailed observation and analysis. The larger deflection and bifurcation of the crack with the local regions are achieved, as shown in Figure 4b, and the fluctuation of the crack can be up to 60 μm . Due to the existence of the equiaxed α phase at the grain boundary, the main crack does not further propagate along the β grain boundary, but changes the direction of propagation away from the GB, even though some microcracks initiate at the equiaxed α interface in front of the crack tip (Figure 4c). This result indicates that the equiaxed α phase at the GB could be the obstacle to the crack growth and lead to branching of the crack of about 90 μm in length. Figure 4d displays the characteristics of the secondary crack initiation near the main crack. It is suggested that although the crack is created at the grain boundary, it connects with the interface crack of intragranular α laths, thus avoiding the propagation along the β grain boundary. It has been reported that cracks tend to grow by passing through rather than cutting the thick α lath [15]. This can be further illustrated by Figure 4e, in which the crack mainly propagates along the long axis of the α laths. Additionally, it deviates from the grain boundary with an angle of 58° when it encounters the equiaxed α phase located at the GB (Figure 4e), which improves the crack growth resistance and is beneficial to improving the fracture toughness of the microstructure. These results indicate that a small amount of equiaxed primary α phases located at the grain boundary is instrumental in the deflection and bifurcation of the main crack propagation.

Figure 5a shows that the interface between the primary α lath and the β_{trans} matrix is the preferable location for crack creation. Cracks mainly form at the α lath interface and propagate along the long axis of the primary α lath, forming cracks related to the orientation of the primary α lath. The width of the primary α lath in the TM is almost equal to the thickness of the grain boundary α , and there are a small number of equiaxed α phases with large sizes at the β grain boundary, as shown in Figure 5b. Figure 5c,d (c and d regions in Figure 5b) represent the plastic deformation behavior of the primary equiaxed α phase at the GB and trimodal β grain boundaries, respectively. The equiaxed α phase at the β grain boundary is relatively soft, and reaches yielding first, producing abundant of slip bands. It has been reported that the multi-slip bands with different orientation are preferably created in the equiaxed primary α phase [27,28]. Cracks easily grew along the slip bands in the equiaxed α phase, because the slip bands provided a low energy channel for crack propagation [29]. As displayed in Figure 5c, there is a certain intersection angle of about 70 degrees between the slip bands in the equiaxed α phase and the direction of the β grain boundary. It changes the propagation direction away from the GB, as the main crack propagation encounters the equiaxed α phase because the slip band is not parallel to the β grain boundary. This result can be validated by Figure 4e. Excellent plastic deformation of the equiaxed α phase results in the blunting effect at the GB, which reduces the crack growth rate [30]. Figure 5d shows that the dislocation slip band occurs both in the GB α phase and the primary α lath, that is, the plastic deformation is not only confined to the GB α phase. At the trimodal β grain boundary, the plastic deformation takes place both at the GB α and the primary α phase near the grain boundary simultaneously, which reduces the local plastic deformation at the grain boundary, making the strain distribution near the grain boundary more uniform, and reducing the strain concentration at β grain boundary to some extent.

Figure 6 shows the plastic deformation and strain distribution in front of the main crack. Three β grains named grain 1, grain 2, and grain 3 are observed in Figure 6a. Several primary α_{p} particles are located at the grain boundary, such as $\alpha_{\text{p}1}$, $\alpha_{\text{p}2}$, $\alpha_{\text{p}3}$, $\alpha_{\text{p}5}$, and $\alpha_{\text{p}7}$ (Figure 6a). Two α_{l} colonies are observed (named colony1 and colony2). From the inverse pole figure (IPF) map of the α phase,

the crystal orientations of α_{p1} to α_{p7} are $(-13 -21)$, $(-4.11 -70)$, $(17 -8 -6)$, $(-12 -10)$, $(17 -80)$, $(-13 -20)$ and $(-12 -1 -1)$, respectively (the direction is perpendicular to the surface). This indicates that the anisotropy displays between these α_p particles. It displays the IPF map of the β grains in Figure 6c, which shows that the crystal orientation for grain 1, grain 2 and grain 3 is (315) , (435) and (546) , respectively. The Schmid factors of basal slip for α_{p1} to α_{p7} are 0.3, 0.11, 0.25, 0.14, 0.36 and 0.5, respectively, while value of colony1 and colony2 is 0.43 and 0.44, respectively (Figure 6d). However, relatively higher Schmid factor values of prismatic slip of the α_p particles are observed in Figure 6e, except for α_{p2} with 0.01 and α_{p7} with 0.25. Additionally, the Schmid factor values for colony1 and colony2 are 0.34 and 0.31, respectively. Figure 6f shows the strain distribution ahead of the crack tip, which indicates that the plastic strain is relatively inhomogeneous and forms a partition with the β grain interior instead of concentrating at the grain boundary. Even if slightly higher strain concentration is observed at the boundaries of colony1 and colony2 in Figure 6f, this strain partition effect effectively avoids the crack initiation and propagation at the grain boundary. Thus, the crack initiation and propagation mainly happens at the boundaries of α_1 colonies within the β grains, as can be seen in Figure 5a.

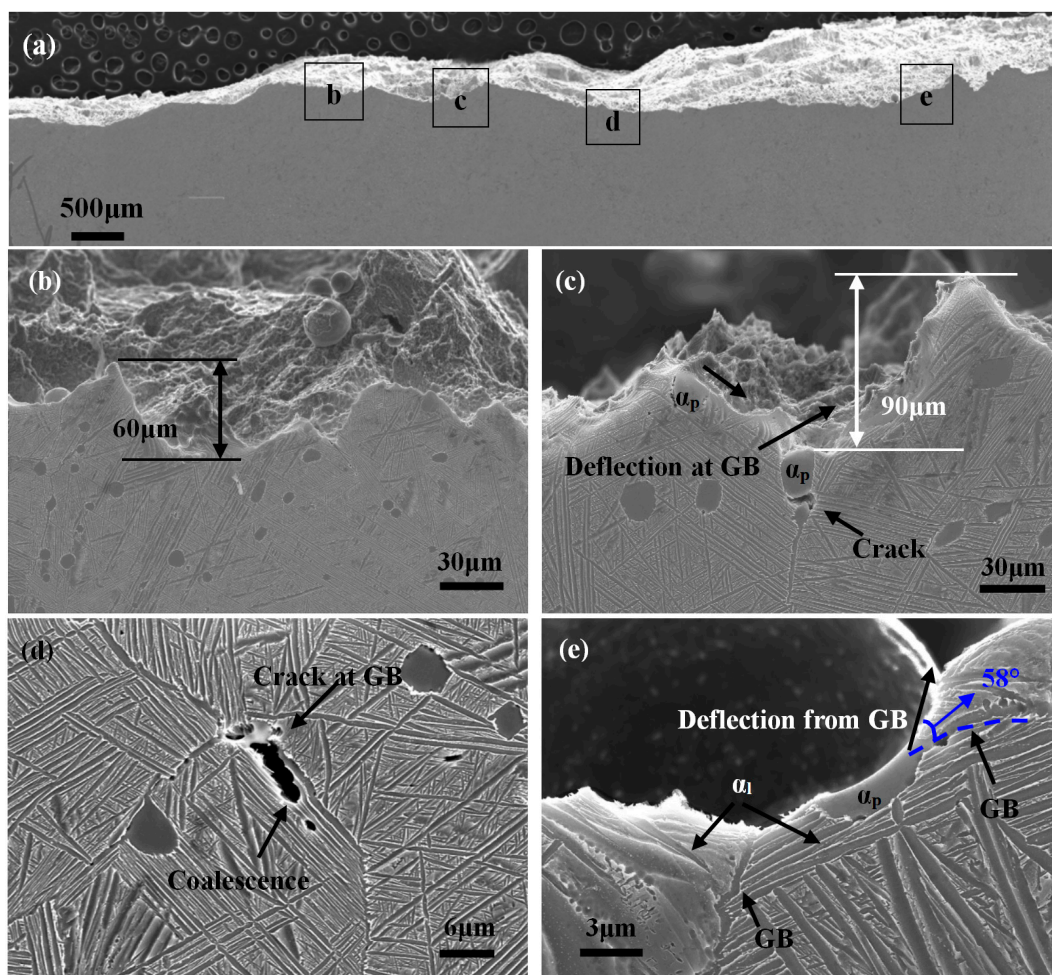


Figure 4. The crack front profiles of the fractured specimen of TM: (a) the propagation path of the main crack; (b) high fluctuation of about 60 μm of the propagation path is observed in microregion, (c) the crack initiates from the α_p interface but not connects with the main crack, which indicates that α_p inhibits the crack growth along the GB; (d) although the crack forms at the GB, it propagates into the grain interior through connecting with the microcrack in α_1 , (e) the main cracks propagate along the grain boundaries and deviate from grain boundaries with about 58° when encounter α_1 and α_p .

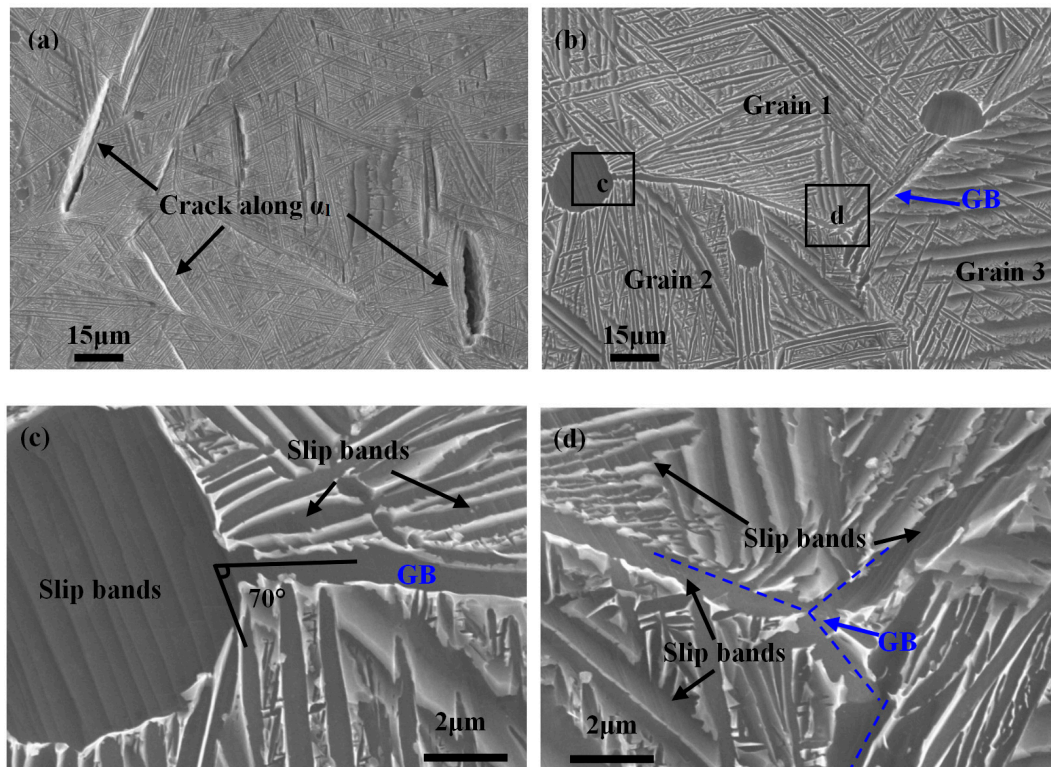


Figure 5. The plastic deformation and crack initiation behavior of the TM: (a) the crack initiates in α_1 ; (b) the equiaxed α phase (α_p) in the β GB; (c) the multi-slip bands in the globular α phase, (d) the dislocation slip bands occur both in the GB α phase and α_1 ; the plastic deformation is not confined to the GB α phase.

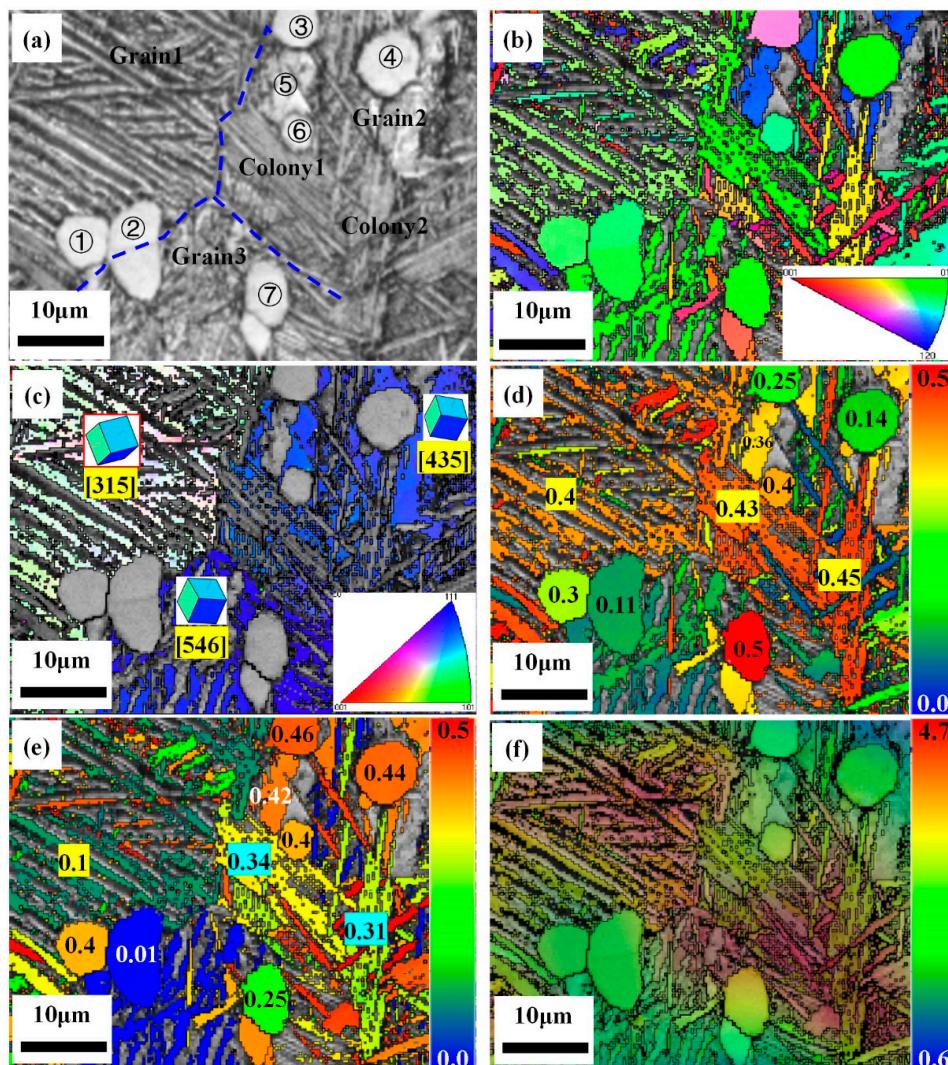


Figure 6. The plastic deformation and strain distribution in front of the main crack: (a) the α_p particles located at the grain boundary; (b) the inverse pole figure (IPF) map of the α phase; (c) the IPF map of the β phase; (d) the Schmid factor of basal slip of the α phase; (e) the Schmid factor of prismatic slip of the α phase; (f) the strain distribution near the grain boundary.

4. Discussion

The main difference of trimodal microstructure is that it contains a small amount of primary equiaxed α phases (about 5% in volume fraction) besides the primary α lath and the β_{trans} matrix. As Chan [30] reported, the softer equiaxed α phase can preferentially coordinate plastic incompatibility and cause blunting of cracks to achieve toughening. Consequently, a certain strain can be produced in the adjacent matrix, and the strain distribution near the grain boundary is more uniform and does not cause the formation of microcracks on the adjacent grain boundary or phase boundary, thus improving the fracture toughness. This can be seen in Figure 5, which shows that the plastic deformation is not only confined to the GB α phase, but occurs both in the α_p phase and the neighbor primary α lath. Based on EBSD, the strain partition within the grain interior that could reduce the stress concentration at the grain boundary to some extent was observed (Figure 6f).

Due to the thick α_1 phase (32.0% in volume fraction), cracks nucleated mainly at the α_1 phase within the grain interior in the trimodal microstructure instead of at the β grain boundary, which was different with the lamellar microstructure or widmannstatten microstructure [31], as shown in Figure 5a. Furthermore, it has been reported that cracks are both deviated and arrested when they reached an

α phase unfavorably oriented for prismatic slip in a two-phase titanium alloy [32]. As can be seen in Figure 6e, a very low Schmid factor value of approximately 0.01 of prismatic slip was obtained in the primary α_{p2} phases. It seems that crack arresting and crack path deviation will happen when the crack tip encounters these unfavorably oriented phases. Retardation of the crack growth occurs due to the crack arresting and deviation, as it requires more energy to expand the crack to a lower stress position, subsequently improving the crack propagation resistance of the trimodal microstructure. As the crack continues to grow, the crack tip tends to stop propagation, blunting or deviate from the grain boundary when it penetrates the equiaxed α phase, as shown in Figure 4c,e. Crack propagation will deflect along the long axis direction of the primary α lath or the direction of slip bands within the equiaxed primary α phase at the grain boundary, avoiding propagation along the β grain boundary and promoting the transgranular fracture. It can be seen that a high fluctuation (up to 90 μm) of the crack path is observed in the microregion of the TM, which increases the flexibility of crack growth and enhances the resistance of crack growth (Figure 4c).

Moreover, although the width of the GB α in the TM is about 640 nm, it displays a distinct characteristic of discontinuous and zig-zag features as marked by the blue dotted lines in Figure 7a. The width and continuity of the GB α can significantly influence the fracture toughness [33]. Researchers have reported that the thicker and continuous GB α would lead to a preferable crack propagation path and induce a detrimental influence on the fracture toughness [4,22]. However, the crack propagation is much more difficult to pass through the discontinuous grain boundary α , which is beneficial to the heightening of fracture toughness [14,33]. In contrast, in the widmannstatten microstructure, because of the lack of toughening effect of the primary equiaxed α phase, cracks are easy to initiate at grain boundaries and propagate along the β grain boundary, which results in low plasticity [31]. According to the present experiments and theoretical analysis, the schematic diagram is carried out to illustrate the effect of α morphology on the crack nucleation and growth behavior of titanium alloy, as shown in Figure 7b. It indicates that the crack mainly initiates at the primary α lath (α_1), and it avoids the initiation of the crack at the β grain boundary. Cracks will change the direction of propagation when they encounter the equiaxed α_p phase at the β grain boundary, which leads to a tortuous crack growth path. This study can provide theoretical support to tailor the microstructure and the mechanical properties of titanium alloys that contain both the α and β phase. For instance, a small number of equiaxed primary α phases are needed if high ductility and fracture toughness are required. It also indicates that a large primary equiaxed α phase is not always detrimental to fracture toughness. If the appropriate amount of the equiaxed α_p phase is obtained, the fracture toughness of the trimodal or bimodal microstructure may be higher than that of the lamellar microstructure.

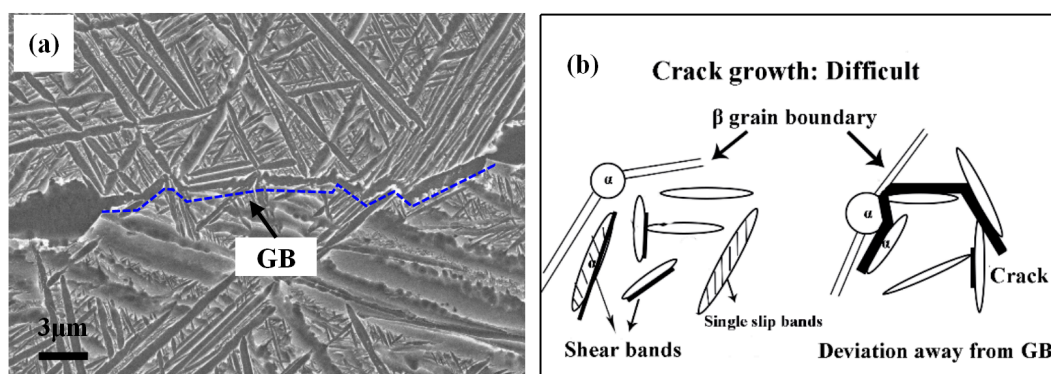


Figure 7. The features of the grain boundary α phase and the schematic diagram of crack growth behavior: (a) the discontinuous and “zig-zag” GB α phase, (b) the crack mainly initiates at α_1 , and it will change the direction of propagation when it encounters the equiaxed α phase at the β grain boundary, which leads to an intergranular fracture.

5. Conclusions

The plastic deformation and crack propagation behavior of the titanium alloy with a trimodal microstructure were systematically investigated during fracture toughness tests. According to the present work, the following conclusions are drawn: A higher fracture toughness of $62 \text{ MPa}\cdot\text{m}^{1/2}$ is obtained for the trimodal microstructure, which offers a preferable combination of strength (1186 MPa) and ductility (12.1%). In addition to dimples, a large number of tearing edges and secondary cracks are produced in the trimodal microstructure, showing transgranular fracture characteristics. The coarser and longer intragranular α lath and a small number of equiaxed α phases, as well as the discontinuous GB α , lead to a high number of branches and fluctuation of the cracks. Because of the toughening effect of the softer phase at the GB, the equiaxed α phase can preferentially coordinate plastic incompatibility and cause arresting and blunting of cracks, which improves the crack growth resistance in the trimodal microstructure. These results indicate that a small amount of the primary globular α phases located at the grain boundary will be good for improving the resistance to crack propagation. The present work can provide a theoretical support to tailor the microstructure and mechanical properties of titanium alloys in the future.

Author Contributions: Conceptualization, C.T. and G.Z.; data curation, C.T. and Q.S.; investigation, C.T. and Y.F.; project administration, G.Z.; supervision, C.T.; visualization, Q.S.; writing—original draft, C.T.; writing—review and editing, Q.S. and G.Z. All authors have read and agreed to the published version of the manuscript.

Funding: This project was financially funded by China Postdoctoral Science Foundation (2020M673614XB), the Natural Science Basic Research Program of Shaanxi (Program No. 2020JQ-618), the State Key Laboratory for Mechanical Behavior of Materials (20202211) and the National Natural Science Foundation of China (Grants No. 51671158 and 51674196).

Conflicts of Interest: The authors declare no conflict of interest.

References

1. Banerjee, D.; Williams, J.C. Perspectives on titanium science and technology. *Acta Mater.* **2013**, *61*, 844–879. [[CrossRef](#)]
2. Leyens, C.; Peters, M. *Titanium and Titanium Alloys: Fundamentals and Applications*; John Wiley & Sons: Hoboken, NJ, USA, 2003.
3. Liu, Y.W.; Chen, F.W.; Xu, G.L.; Cui, Y.W.; Chang, H. Correlation between Microstructure and Mechanical Properties of Heat-Treated Ti-6Al-4V with Fe Alloying. *Metals* **2020**, *10*, 854. [[CrossRef](#)]
4. Renon, V.; Henaff, G.; Larignon, C.; Perusin, S.; Villechaise, P. Identification of Relationships between Heat Treatment and Fatigue Crack Growth of $\alpha\beta$ Titanium Alloys. *Metals* **2019**, *9*, 512. [[CrossRef](#)]
5. He, S.T.; Zeng, W.D.; Xu, J.W.; Chen, W. The effects of microstructure evolution on the fracture toughness of BT-25 titanium alloy during isothermal forging and subsequent heat treatment. *Mater. Sci. Eng. A* **2019**, *745*, 203–211. [[CrossRef](#)]
6. Niinomi, M.; Kobayashi, T.; Inagaki, I.; Thompson, A.W. The effect of deformation-induced transformation on the fracture toughness of commercial titanium alloys. *Metall. Trans. A* **1990**, *21*, 1733–1744. [[CrossRef](#)]
7. Li, X.H.; He, J.C.; Ji, Y.J.; Zhang, T.C.; Zhang, Y.H. Study of the Microstructure and Fracture Toughness of TC17 Titanium Alloy Linear Friction Welding Joint. *Metals* **2019**, *9*, 430. [[CrossRef](#)]
8. Xu, T.W.; Zhang, S.S.; Cui, N.; Cao, L.; Wan, Y. Precipitation Behavior of Ti15Mo Alloy and Effects on Microstructure and Mechanical Performance. *J. Mater. Eng. Perform.* **2019**, *28*, 7188–7197. [[CrossRef](#)]
9. Wen, X.; Wan, M.P.; Huang, C.W.; Tan, Y.B.; Lei, M.; Liang, Y.L.; Cai, X. Effect of microstructure on tensile properties, impact toughness and fracture toughness of TC21 alloy. *Mater. Des.* **2019**, *180*, 107898. [[CrossRef](#)]
10. Shi, X.H.; Zeng, W.D.; Zhao, Q.Y. The effects of lamellar features on the fracture toughness of Ti-17 titanium alloy. *Mater. Sci. Eng. A* **2015**, *636*, 543–550. [[CrossRef](#)]
11. Wen, X.; Wan, M.P.; Huang, C.W.; Lei, M. Strength and fracture toughness of TC21 alloy with multi-level lamellar microstructure. *Mater. Sci. Eng. A* **2019**, *740*, 121–129. [[CrossRef](#)]
12. Richards, N.L. Quantitative evaluation of fracture toughness-microstructural relationships in α - β titanium alloys. *J. Mater. Eng. Perform.* **2004**, *13*, 218–225. [[CrossRef](#)]

13. Cvijović-Alagić, I.; Gubelj, N.; Rakin, M.; Cvijović, Z.; Gerić, K. Microstructural morphology effects on fracture resistance and crack tip strain distribution in Ti-6Al-4V alloy for orthopedic implants. *Mater. Des.* **2014**, *53*, 870–880. [[CrossRef](#)]
14. Fan, J.K.; Li, J.S.; Kou, H.C.; Hua, K.; Tang, B. The interrelationship of fracture toughness and microstructure in a new near β titanium alloy Ti-7Mo-3Nb-3Cr-3Al. *Mater. Charact.* **2014**, *96*, 93–99. [[CrossRef](#)]
15. Hirth, J.P.; Froes, F.H. Interrelations between fracture toughness and other mechanical properties in titanium alloy. *Metall. Trans. A* **1977**, *8A*, 1165–1176. [[CrossRef](#)]
16. Gao, P.F.; Cai, Y.; Zhan, M.; Fan, X.G.; Lei, Z.N. Crystallographic orientation evolution during the development of tri-modal microstructure in the hot working of TA15 titanium alloy. *J. Alloys Compd.* **2018**, *741*, 734–745. [[CrossRef](#)]
17. Gao, P.F.; Fan, X.G.; Yang, H. Role of processing parameters in the development of tri-modal microstructure during isothermal local loading forming of TA15 titanium alloy. *J. Mater. Process. Technol.* **2017**, *239*, 160–171. [[CrossRef](#)]
18. Hosseini, R.; Morakabati, M.; Abbasi, S.M.; Hajari, A. Development of a trimodal microstructure with superior combined strength, ductility and creep-rupture properties in a near α titanium alloy. *Mater. Sci. Eng. A* **2017**, *696*, 155–165. [[CrossRef](#)]
19. Tan, C.S.; Sun, Q.Y.; Zhang, G.J. Role of microstructure in plastic deformation and crack propagation behaviour of an α/β titanium alloy. *Vacuum* **2020**, major revise.
20. Zhang, S.; Liang, Y.L.; Xia, Q.F.; Ou, M.G. Study on Tensile Deformation Behavior of TC21 Titanium Alloy. *J. Mater. Eng. Perform.* **2019**, *28*, 1581–1590. [[CrossRef](#)]
21. Jia, R.C.; Zeng, W.D.; He, S.T.; Gao, X.X.; Xu, J.W. The analysis of fracture toughness and fracture mechanism of Ti60 alloy under different temperatures. *J. Alloys Compd.* **2019**, *810*, 151899. [[CrossRef](#)]
22. Terlinde, G.; Rathjen, H.J.; Schwalbe, K.H. Microstructure and fracture toughness of the aged, β -Ti Alloy Ti-10V-2Fe-M. *Metall. Trans. A* **1988**, *19*, 1037–1049. [[CrossRef](#)]
23. Niinomi, M.; Kobayashi, T. Fracture characteristics analysis related to the microstructures in titanium alloys. *Mater. Sci. Eng. A* **1996**, *213*, 16–24. [[CrossRef](#)]
24. Ren, L.; Xiao, W.L.; Chang, H.; Zhao, Y.Q.; Ma, C.L.; Zhou, L. Microstructural tailoring and mechanical properties of a multi-alloyed near β titanium alloy Ti-5321 with various heat treatment. *Mater. Sci. Eng. A* **2018**, *711*, 553–561. [[CrossRef](#)]
25. Suresh, S. Fatigue crack deflection and fracture surface contact: Micromechanical models. *Metall. Trans. A* **1985**, *16*, 249–260. [[CrossRef](#)]
26. Xu, J.W.; Zeng, W.D.; Zhou, D.D.; Ma, H.Y.; Chen, W.; He, S.T. Influence of α/β processing on fracture toughness for a two-phase titanium alloy. *Mater. Sci. Eng. A* **2018**, *731*, 85–92. [[CrossRef](#)]
27. Tan, C.S.; Sun, Q.Y.; Xiao, L.; Zhao, Y.Q.; Sun, J. Cyclic deformation and microcrack initiation during stress controlled high cycle fatigue of a titanium alloy. *Mater. Sci. Eng. A* **2018**, *711C*, 212–222. [[CrossRef](#)]
28. Huang, J.; Wang, Z.R.; Xue, K.M. Cyclic deformation response and micromechanisms of Ti alloy Ti-5Al-5V-5Mo-3Cr-0.5Fe. *Mater. Sci. Eng. A* **2011**, *528*, 8723–8732. [[CrossRef](#)]
29. Sangid, M.D. The physics of fatigue crack initiation. *Int. J. Fatigue* **2013**, *57*, 58–72. [[CrossRef](#)]
30. Chan, K.S. Toughening mechanisms in titanium aluminides. *Metall. Trans. A* **1993**, *24A*, 569–583. [[CrossRef](#)]
31. Ankem, S.; Greene, C.A. Recent developments in microstructure: Property relationships of beta titanium alloys. *Mater. Sci. Eng. A* **1999**, *263*, 127–131. [[CrossRef](#)]
32. Bantounas, I.; Lindley, T.C.; Rugg, D.; Dye, D. Effect of microtexture on fatigue cracking in Ti-6Al-4V. *Acta Mater.* **2007**, *55*, 5655–5665. [[CrossRef](#)]
33. Ghosh, A.; Sivaprasad, S.; Bhattacharjee, A.; Kar, S.K. Microstructure–fracture toughness correlation in an aircraft structural component alloy Ti-5Al-5V-5Mo-3Cr. *Mater. Sci. Eng. A* **2013**, *568*, 61–67. [[CrossRef](#)]

